Bioactive Materials 14 (2022) 52–60

Contents lists available at ScienceDirect

Bioactive Materials

journal homepage: www.keaipublishing.com/en/journals/bioactive-materials

An adhesive and resilient hydrogel for the sealing and treatment of gastric perforation

Jing Chen [a,b], Julia S. Caserto [c], Ida Ang [d], Kaavian Shariati [b], James Webb [b], Bo Wang [b], Xi Wang [b], Nikolaos Bouklas [d], Minglin Ma [b,*]

[a] College of Pharmacy, Nanjing University of Chinese Medicine, Nanjing, 210023, China
[b] Department of Biological and Environmental Engineering, Cornell University, Ithaca, NY, 14853, USA
[c] Robert Frederick Smith School of Chemical and Biomolecular Engineering, Cornell University, Ithaca, NY, 14853, USA
[d] Sibley School of Mechanical and Aerospace Engineering, Cornell University, Ithaca, NY, 14853, USA

ARTICLE INFO

Keywords:
Adhesive hydrogel plug
Gastric perforation
Thermo-responsive
Regeneration

ABSTRACT

Adhesive hydrogels have been recently proposed as a potential option to seal and treat gastric perforation (GP) which causes high mortality despite advancements in surgical treatments. However, to be effective, the hydrogels must have sufficient tissue adhesiveness, tough mechanical property, tunable biodegradability and ideally are easy to apply and form. Herein, we report an adhesive and resilient hydrogel for the sealing and treatment of gastric perforation. The hydrogel consists of a bioactive, transglutaminase (TG)-crosslinked gelatin network and a dynamic, borate-crosslinked poly-N-[Tris(hydroxymethyl)methyl]acrylamide (PTH) network. The hydrogel can be formed *in situ*, facilitating easy delivery to the GP and allowing for precise sealing of the defects. *In vivo* experiments, using a perforated stomach mouse model, shows that the adhesive hydrogel plug effectively seals GP defects and promotes gastric mucosa regeneration. Overall, this hydrogel represents a promising biomaterial for GP treatment.

1. Introduction

Peptic ulcer disease (PUD) affects 4 million people worldwide annually [1]. Gastric perforation (GP) is a serious complication of PUD [2,3]. Once perforation occurs in the stomach, it can lead to severe peritonitis after bacteria, stomach acid, and partially digested food enters the abdominal cavity [4–6]. Meanwhile, several complications are often associated with GP including bleeding, sepsis, multi-organ failure, bowel infarction, and wound infection [7], which can exacerbate the condition and accounts for more than 70% of deaths associated with PUD [8]. Surgical intervention in the form of exploratory laparotomy was the initial therapy for GP [9–11]. Despite improvements in surgical and medical treatments, the mortality rate for GP is 30%, while the mortality rate for cases compounded by diffuse peritonitis is up to 70% [12]. Furthermore, sutures require delicate control and prolonged time for application, which is problematic in emergency circumstances [13]. In addition, existing medical glues have significant drawbacks. For example, cyanoacrylate glue exhibits low biocompatibility, difficult handling, and poor integration with stomach tissues [14]. Fibrin glue can stop bleeding, but often suffers from weak adhesion, poor mechanical properties and short degradation time [15,16]. To address these problems, new easy-to-apply biomaterials with strong adhesion, tough mechanical properties, and tunable biodegradability are highly desirable in clinical settings.

Unlike cell sheets that need delicate manipulation to maintain live cells [17–19], cell-free adhesive hydrogels represent a promising candidate for GP treatment. For example, dry double-sided hydrogel tape was made from a combination of a biopolymer (gelatin or chitosan) and crosslinked poly(acrylic acid) grafted with N-hydrosuccinimide ester [15], which provided a fluid-tight sealing of a fluid-filled perforated pig stomach by covalent crosslinking with amine groups on the tissue surface. However, more *in vivo* work needs to be done to further demonstrate its potential for clinical applications. Moreover, poly (N-acryloyl 2-glycine) hydrogels were developed to bond perforated stomach surface via multiple hydrogen bonding interaction [20]. The rabbits treated with the hydrogels all survived, while a 44.4% mortality

Peer review under responsibility of KeAi Communications Co., Ltd.
* Corresponding author.
E-mail address: mm826@cornell.edu (M. Ma).

https://doi.org/10.1016/j.bioactmat.2021.11.038
Received 9 October 2021; Received in revised form 15 November 2021; Accepted 16 November 2021
Available online 17 December 2021

rate was observed after treatment with surgical sutures. However, it was unclear whether the pre-made hydrogel patch was sufficiently adaptable to the stomach tissue. In order to make the hydrogel adaptive to the local biological environment, injectable hydrogel based on supramolecular assembly of an ABA triblock copolymer was applied to the gastric perforation site of rats [21]. It reduced infiltration of inflammatory cells and enhanced vascularization, but mucosa regeneration, critical for optimal GP treatment, was not investigated. Since the stomach tissue is highly stretchable, considering all these and other recent advances [22–26], it is clear that an ideal biomaterial for GP treatment must at least satisfy the following requirements: (i) strong adhesion to the stomach tissue and adaptable to its dynamic movement (ii) stable mechanical properties with appropriate toughness, (iii) high bioactivity and tunable biodegradability, matching endogenous tissue regeneration and (iv) ease of application and use in clinical settings.

Here, we report an *in-situ*-formed, gelatin-based, thermo-responsive, adhesive and tough hydrogel plug that meets all abovementioned requirements for GP treatment. The adhesive plug can be formed after the components are extruded out of a micromixer connected to a dual syringe (with one syringe containing polymers and the other crosslinkers. (Fig. 1A). After mixing and *in situ* crosslinking, two interpenetrating networks are formed. The total amount of interfacial toughness (Γ) is often quantified as the sum of intrinsic toughness (Γ_0) required to break interfacial bonds and energy dissipation in the adhesive hydrogel matrix (Γ_A), which can be expressed as $\Gamma = \Gamma_0 + \Gamma_A$ [27]. The primary network consists of gelatin crosslinked with transglutaminase (TG), which serves as a bioactive, thermo-responsive and adhesive unit, and thus makes contribution to Γ_0. Considering the intrinsic hydrogen bonding in gelatin allowing for dissipation of energy, the primary network may directly enhance both Γ_0 and Γ_A. The secondary network is made of a special triple hydrogen bonding cluster polymer, poly(N-[Tris(hydroxymethyl)methyl] acrylamide) or PTH (Figs. S1 and S2) crosslinked with borate. This network is dynamically crosslinked, which favors dissipation of energy and improves not only the mechanical properties but also the adhesive strength of the whole system by the enhancement of Γ_A. The resulting hydrogel is easily applicable to the GP site and, due to its adhesive, tough, adaptable, degradable and bioactive properties, effectively seals GP defects and

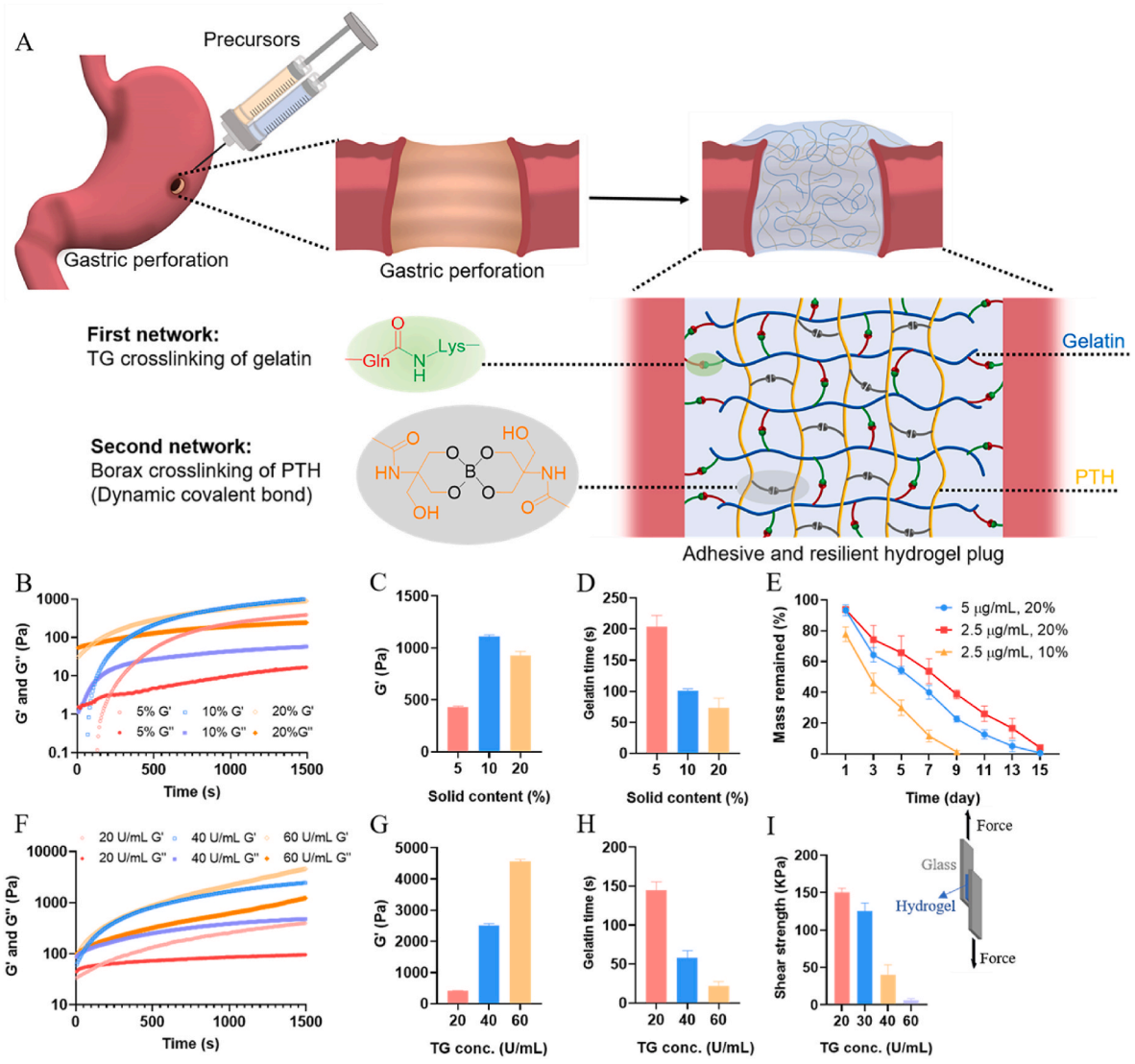

Fig. 1. A) Scheme of an adhesive and resilient hydrogel for the sealing and treatment of gastric perforation. B) Hydrogels crosslinked by 30 U/mL TG with different solid contents of gelatin were examined by a time sweep. C) loss modulus (G′) and D) gelation time of hydrogels. E) *In vitro* degradation of 10% and 20% gelatin hydrogels crosslinked by 30 U/mL TG, in different concentrations of collagenase type II solution in PBS and 37 °C over time. F) 20% gelatin hydrogels crosslinked by different concentrations of TG were examined by a time sweep. G) loss modulus (G′) and H) gelation time of hydrogels. I) Shear strength of 20% gelatin hydrogels crosslinked by different concentrations of TG.

promotes gastric mucosa regeneration in mice.

2. Materials and methods

2.1. Materials

N-[Tris(hydroxymethyl)methyl]acrylamide (THMA, 93%), gelatin, collagenase type II and Ammonium persulfate (APS, 98%) were purchased from Sigma-Aldrich, Transglutaminase was purchased from Moo Gloo.

2.2. Synthesis of PTH

PTH was synthesized by a free radical polymerization method [28]. THMA (910 mg, 5.2 mmol) was dissolved into 6 mL of D.I. water under nitrogen atmosphere. Then APS (23 mg, 0.1 mmol) was added to initiate the polymerization at 60 °C. After 1 h, the temperature was adjusted to 70 °C for further 12 h. After the reaction, PTH was obtained by dialysis (Spectra/Pore, molecular weight cut off (MWCO) of 3500) in D.I. water followed by freeze-drying. ^{1}H NMR (400 MHz, D_2O, Fig. S2, δ): CH and CH_2 on polymer chain: 3.82.

2.3. Rheological testing

The shear storage modulus (G′) and shear loss modulus (G″) over time range of 0–1500 s were measured with a strain of 0.1%. The gelation time was considered as the time when G′ exceed G''. All measurements were repeated three times and taken at a temperature of 37 °C utilizing a 20.0 mm aluminum peltier plate to simulate rheological behavior *in vivo*. All data was analyzed using TA Instruments Trios software and plotted using Graphpad Prism.

2.4. Fabrication of adhesive hydrogels

A certain amount of gelatin (mixed with PTH) and TG (mixed with 0.4 mM of borax) with 1:1 (v/v) ratio was first separately infused inside a 3 mL dual-syringe (Merlin Packaging Technologies, Inc.) which was connected with a micro-mixer and incubated into 37 °C water bath, then they could be injected into mold to fabricate the adhesive hydrogels.

2.5. In vitro enzymatic degradation of the gelatin hydrogels

The *in vitro* degradation of gelatin hydrogels was examined as described previously [29]. Disc-shaped gelatin hydrogel samples (d = 6 mm; h = 3 mm) were formed as previously described. Next, the initial weights of the samples were measured, and the samples were incubated in different concentrations (2.5 and 5 μg/mL) of collagenase type II in PBS for 1, 3, 5, 7, 9, 11, 13 and 15 days. At each time point, the final weights of samples after being dried were measured. The degradation percentage of each sample was calculated based on weight loss over time.

2.6. Mechanical property testing

The GTx-PTHy hydrogels were prepared in a cylindrical shape (D = 15 mm, H = 10 mm) for compression testing and a rectangular shape (L = 5 mm, W = 30 mm) for tensile testing. The mechanical property measurements of the hydrogels were performed using a universal testing machine (Instron, America) with a 100 N load cell. The compressive tests were measured at a speed of 1 mm/min with a compression of 90%. The tensile test of the hydrogel was performed at an extension speed of 10 mm/min. The fracture energy was tested using a classical single-edge notch test according to a previous study [30]. The data were determined based on the average of three measurements.

2.7. Adhesion tests

Shear stress testing was performed to measure the shear strength of the GTx-PTHy hydrogels to glass slides. The hydrogels were applied to the glass surface with a square bond area of 25 mm × 25 mm. The samples were pulled to failure using a universal testing machine (Instron, USA) with a cross-head speed of 5 mm/min under ambient conditions. The adhesive strength was determined as the maximum shear stress based on the average of three measurements.

2.8. 2D cell seeding on adhesive hydrogels

First, 500 μL of hydrogel was injected into each well (Corning, 24 well). Next, 50 μL of MSCs (Strain C57BL/6 Mouse Mesenchymal Stromal Cells (Cyagen, MUBMX-01001, P10)) suspension (2×10^6 cells/mL) were seeded on each sample. After 45-min incubation, 360 μL of cell culture media was added to each sample and maintained at 37 °C and 5% CO_2 for 3 days. In addition, cells at the same density were also seeded inside 24-well tissue culture plates. The cells were visualized by LIVE/DEAD staining and the pictures were subsequently captured by fluorescent microscope (EVOS FL Cell Imaging System) according to previous reported [31]. Quantification of the percentage of live cells was carried out by calculating the intensity of fluorescence using ImageJ.

2.9. 2D cell scratch test

The adhesive hydrogel was prepared as previously described. 500 μL of hydrogel was injected into each well. Then MSCs (2×10^6 cells/ml) were seeded on the hydrogels and maintained at 37 °C and 5% CO_2. After 2 days, the cell layer on the surface of the hydrogels was scratched using a 1-ml pipette tips. The cells were stained at day 0, 1, 2 and 3 after creating the scratch. Polystyrene 24-well plates were used as control. Quantification of the percentage of live cells was carried out by calculating the intensity of fluorescence using ImageJ.

2.10. In vitro cytocompatibility assay

MSCs were plated in a 96-well plate (1×10^4 cells/well) in an atmosphere containing 5% CO_2 for 24 h at 37 °C. The 100 μL of adhesive hydrogels were applied to each well. After 1, 4 and 7 days 3-(4,5-dimethylthiazol-2-yl)-2,5-diphenyl tetrazoliumbromide (MTT) solution in PBS (10 μL, 5 mg/mL) was added. After incubation for 4 h, the supernatant was carefully aspirated, and the MTT-formazan generated by live cells was dissolved in 150 μL of DMSO for 20 min. Absorbance at a wavelength of 490 nm was measured using a microplate reader (Bio-Tek, ELX808IU). Relative cell viability (%) was determined by comparing absorbance at 490 nm with control wells containing only cell culture medium. The experiments were performed in quartets, and data were presented as an average ± SD.

2.11. Simulation method

We conducted simulations to further examine the properties of the GT20-PTH10 (where 20 denoted the mass fraction of gelatin (i.e. weight of gelatin/weight of water), and 10 denoted the mass fraction of PTH.) hydrogel, which exhibits a low stiffness but high adhesion at 37 °C. The typical stomach volume of the mice used for the *in vivo* GP study ranges from 1.5 to 2 mL, and the maximum volume that can be infused into the stomach is approximately 0.1 mL. Therefore, we modeled the stomach as a hollow sphere with inner radius 7.10 mm and thickness of 0.5 mm, corresponding to literature values of the stomach wall thickness [32]. A mixed finite element formulation for displacements and pressures was implemented in FEniCS [33,34], where the hyperelastic incompressible neo-Hookean material model was used (see supplemental). The material properties of the GT20-PTH10 hydrogel can be determined by assuming the material is close to incompressiblity, Poisson's ratio of 0.49, and

determining the Young's modulus from the stress-strain curves in Fig. 2A. This calculation yields a shear modulus of 18.2 Pa for the hydrogel, and the shear modulus of a rat's stomach was found from literature to be 2.86E4 Pa [32]. For the first step, the hollow sphere modeled with the stomach material properties was prescribed an inner displacement to expand the sphere to an inner radius of 8.31 mm. This value is consistent with nine times the infusion volume, 0.9 mL, to examine stretches past the physiological limit. This displacement is then applied to the inner boundary of a dual material setup, and the nominal stresses and stretches on the plug surface can be determined from the displacements and pressures that are found from the simulation.

2.12. GP treatment in vivo

All animal studies were approved by the Cornell Institutional Animal Care and Use Committee and anesthetized using 3% isoflurane in oxygen and maintained at the same rate throughout the procedure. A ~5-mm incision was made above the stomach. After creating an approximately 5 mm diameter hole, a sterile paper towel was used to remove the blood and then the gelatin (mixed with PTH) and TG (mixed with borax), separately infused inside a dual-syringe and incubated into 37 °C water bath, were injected into the hole. The mixture was held in place within the hole by tweezers and subsequently underwent gelation to form a plug to block the hole. The incision was closed using 5–0 taper polydioxanone (PDS II) absorbable sutures. The mice were euthanized at desired time points post implantation to acquire the stomach tissues. They were then transferred into 4% paraformaldehyde for fixation.

2.13. Histological analysis

At the end of the treatment, mice of all groups were euthanized, and the stomachs were excised. Then they were fixed with 4% paraformaldehyde solution and embedded in paraffin. The sliced tissues mounted on the glass slides were stained by hematoxylin and eosin (H&E) and observed by digital microscope (Leica Q Win).

2.14. Statistical analysis

All statistical analysis was performed with GraphPad Prism 9. Ordinary One-way ANOVA test with Tukey's post hoc test was used to determine statistical significance between GT20 and GT20-PTH10 hydrogels for mechanical and adhesion characterization. Ordinary Two-way ANOVA test with Sidak's post hoc test was used to determine statistical significance for comparison of two groups for cell experiments, respectively. Unpaired *t*-test was used to determine statistical significance for gastric mucosa thickness after two treatments.

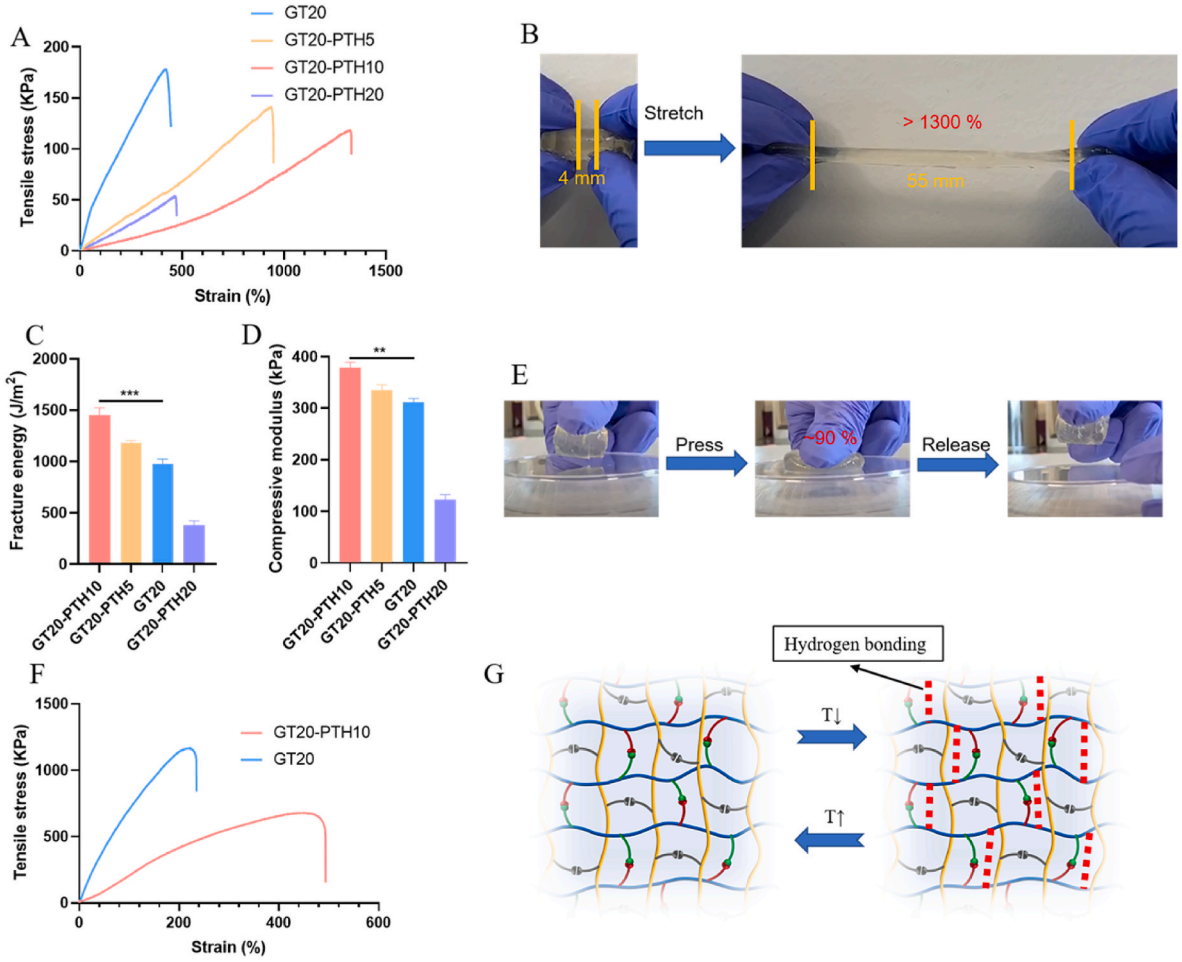

Fig. 2. A) Typical tensile stress-strain curves of the double network hydrogel: 20% gelatin hydrogel crosslinked by 20 U/mL TG as a first network and different contents of PTH crosslinked by 0.4 mM of borax as a secondary network under 37 °C. B) The GT20-PTH10 hydrogel was elongated to 13 times its initial length under 37 °C. C) Fracture energy of GT20-PTHy, y varied from 0 to 20 and D) corresponding compressive modulus of different hydrogels. E) The GT20-PTH10 hydrogel was compressed to 90% and recovered immediately. F) Tensile stress-strain curves of the GT20-PTH10 and GT20 hydrogels under 25 °C. G) Scheme of inter-network of GT20-PTHy hydrogels undergoing reverse temperature change.

3. Results and discussion

3.1. Optimization of adhesive primary network

To make the adhesive plug dynamically adaptable and deformable to stomach tissue, we first screened the optimal ratio of gelatin and TG to make an adhesive primary network with relatively short and operable gelation time. When the TG concentration was fixed to 30 U/mL, the maximum elastic modulus (G′), measured using a rheology test, increased with increasing solid gelatin content from 5% to 10% (weight of gelatin/weight of water) and then decreased when the solid content reached 20% (Fig. 1B). A maximum G′ of 1112 Pa was achieved for the hydrogel with 10% gelatin (Fig. 1C), which was greater than that of 20% and 5% gelatin (927.7 and 426.3 Pa, respectively). However, the gelation time was largely reduced with increased gelatin solid content, achieving the shortest time of 73s with 20% gelatin content (Fig. 1D). Enzymatic degradation of the 10% and 20% gelatin hydrogels crosslinked with 30 U/mL of TG was also characterized (Fig. 1E). The enzymatic degradation of gelatin hydrogels was measured by incubation in different collagenase type II solutions (2.5 and 5 μg/mL in PBS) for up to 15 days. Results showed that the collagenase concentration directly affected *in vitro* degradation rate of the gelatin hydrogels. For the 20% gelatin hydrogel, 5 μg/mL collagenase showed 94.9% degradation after 13 days of incubation, while 83.3% degradation was obtained for 2.5 μg/mL collagenase. The degradation could be further accelerated by reducing the gelatin content. For the 10% gelatin hydrogel, it showed 98.8% degradation after 9 days of incubation. Considering that the high gelatin content would favor more retention time *in vivo,* we chose 20% gelatin content and varied the TG concentration for further experimentation. Even though higher TG concentrations (40 U/mL and 60 U/mL) resulted in higher G' of 2511 and 4576 Pa (Fig. 1F & G) and lower gelation times of 58 and 22 s (Fig. 1H), shear strengths (evaluated by a lap-shear test) of the hydrogels from the higher TG concentrations were much lower than the 20 U/mL group (Fig. 1I). Therefore, 20% gelatin solid content with 20 U/mL of TG was chosen for further experiments.

3.2. Mechanical properties

An optimal gastrointestinal sealant biomaterial should be elastic enough to allow for peristaltic movements [35,36]. In order to enhance the mechanical properties as well as adhesive strength of the gelatin hydrogel, PTH dynamically crosslinked by 0.4 mM of borax was incorporated as a secondary network. The resultant hydrogels were named as GTx-PTHy, where x denoted the mass fraction of gelatin (i.e. weight of gelatin/weight of water), and y denoted the mass fraction of PTH. Fig. 2A shows the typical tensile stress-strain curves of the hydrogels under tensile tests. The maximum tensile strain under 37 °C increased with PTH content and reached a maximum value of 1323% at 10%, much higher than that of the GT20-PTH5 hydrogel (938%), and in sharp contrast to that of the GT20 and GT20-PTH20 hydrogels (419% and 467%, respectively). These results demonstrated that the GT20-PTH10 hydrogel was sufficiently stretchable and tough. It is worthy to note that its maximum tensile strain was higher than previously reported adhesive hydrogels for GP treatment [20–22,26,36]. As shown in Fig. 2B, the GT20-PTH10 hydrogel was stretched 13 times its initial length (Video V1). The fracture energy showed a similar trend, as demonstrated by the single edge notched tests (Fig. 2C). A maximum fracture energy of 1450 J/m^2 was achieved for the GT20-PTH10 hydrogel. Meanwhile, its compressive modulus (378 KPa) was higher than that of GT20 (311 KPa) without any PTH addition (Fig. 2D). It also withstood a high compression to complete deformation without breaking. After the compressive load was removed, the GT20-PTH10 hydrogel recovered rapidly to its initial shape (Fig. 2E and Video V2). However, the maximum tensile strain of GT20-PTH10 hydrogel under 25 °C reduced to 469%, in contrast to that of GT20 (221%) (Fig. 2F). This highlights the wide range of controllable mechanical properties, which can be obtained by changing temperature. When the temperature was increased to 37 °C, the hydrogen bonds between gelatin polymer chains were broken allowing more stretch, but these bonds could be reversibly reformed when the temperature was reduced to 25 °C (Fig. 2G).

Supplementary video related to this article can be found at https://doi.org/10.1016/j.bioactmat.2021.11.038

The shear strength of the hydrogels under 37 °C increased with the ratio of PTH from 0 to 10% (Fig. 3A), with the maximum reaching 251 KPa at PTH10 (Fig. 3B). However, the shear strength reduced to 163 KPa when PTH further increased to 20%. The GT20-PTH10 hydrogel strongly adhered to a rubber glove and plastic cell culture lid with a clear adhesion interface after lifting the hydrogel (Fig. 3C). However, nothing remained at the surface of the plastic lid, indicating its high adhesive and mechanical strength (Video V3). Meanwhile, adhesion could be adjusted according to temperature. When the temperature was reduced from 37 °C to 25 °C, the shear strength reduced to almost zero (Fig. 3D). If we repeated the cycle, the shear strength could be maintained for almost 60 cycles with only slight reduction. Lastly, we confirmed the GT20-PTH10 hydrogel was highly adhesive to biological tissues including the stomach, liver, kidney, heart, and spleen (Fig. 3E). The GT20-PTH10 hydrogel reached an equilibrium swollen state after ~72 h of immersion in PBS at 37 °C with a swelling ratio of 5.15 (Fig. S3).

Supplementary video related to this article can be found at https://doi.org/10.1016/j.bioactmat.2021.11.038

3.3. Cyto-compatibility of GT20-PTH10 adhesive hydrogel

Ideally, an adhesive hydrogel for GP treatment should present no cytotoxicity. It should also permit cells of the injured tissue to migrate into the adhesive hydrogel for long-term cell integration and repair [37–39]. Therefore, we aimed to evaluate the *in vitro* cyto-compatibility and cell migration potential for the engineered adhesive hydrogel using 2D cell seeding and scratch tests [40]. To accomplish this, the cyto-compatibility of the GT20-PTH10 hydrogel was assessed *in vitro*. The viability, adhesion, and proliferation activity of MSCs seeded on the adhesive hydrogel were evaluated using a commercial kit for LIVE/-DEAD assays and MTT tests. The results were compared to the viability of cells seeded on tissue culture plates, which served as the control. The results showed that the cells seeded on tissue culture plates and GT20-PTH10 adhesive hydrogels both exhibited high viability (>100%) 2 and 3 days after seeding (Fig. 4A). The MTT quantification of cell viability also confirmed this observation (Fig. 4B). The *in vitro* scratch assay revealed that MSCs seeded on the surface of both well plates and GT20-PTH10 adhesive hydrogel could migrate to the scratched area within 24 h (Fig. 4C). To quantify the migration to the “wounded” area, we compared cell density in the scratched area to the surrounding cell density. The results showed that the relative cell density for the GT20-PTH10 adhesive hydrogel was higher than that of the control (tissue culture plate) 2 and 3 days after creating the scratch (Fig. 4D). For example, the relative cell density for GT20-PTH10 adhesive hydrogel was 100 ± 5%, which was higher than the control (92 ± 3% for culture plate) after 3 days. This indicated that GT20-PTH10 adhesive hydrogel could facilitate cell migration and proliferation.

3.4. Simulation and GP treatment with GT20-PTH10 adhesive hydrogel

Before applying the hydrogel to the stomach surface and test its potential for GP treatment, we did simulation to calculate the interfacial stress after application of the hydrogel plug to the GP in a mouse stomach. The displacement on the inner surface is increased uniformly to a final radial stretch of $\lambda_r = 1.16$ corresponding to an infusion volume of 0.9 mL (Fig. 5A). Throughout each stage of the simulation, the adhesive hydrogel, which is softer than the native stomach tissue, experiences the lowest nominal stress magnitude, |P|. At the final

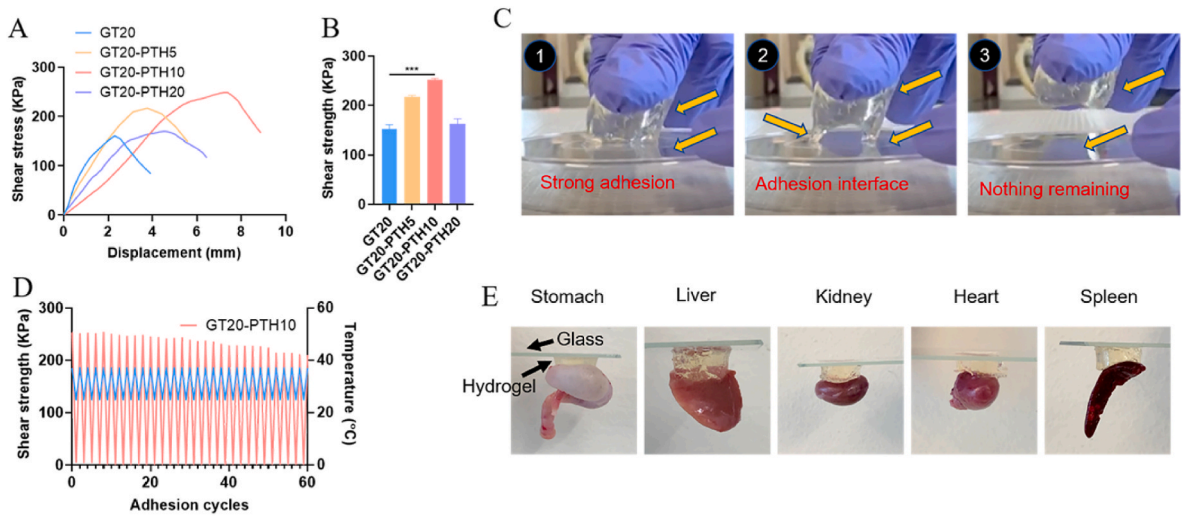

Fig. 3. A) Typical shear stress curves of different hydrogels to a glass slide under 37 °C and B) corresponding shear strength (n = 3). C) Optical images of the GT20-PTH10 hydrogel sticking to the lid of cell culture dish and the adhesion interface when being lifted under 37 °C. D) Reversible adhesion property of GT20-PTH10 hydrogel under 37 °C and 25 °C. E) The GT20-PTH10 hydrogel adhered to various tissue surfaces including the stomach, liver, kidney, heart, and spleen.

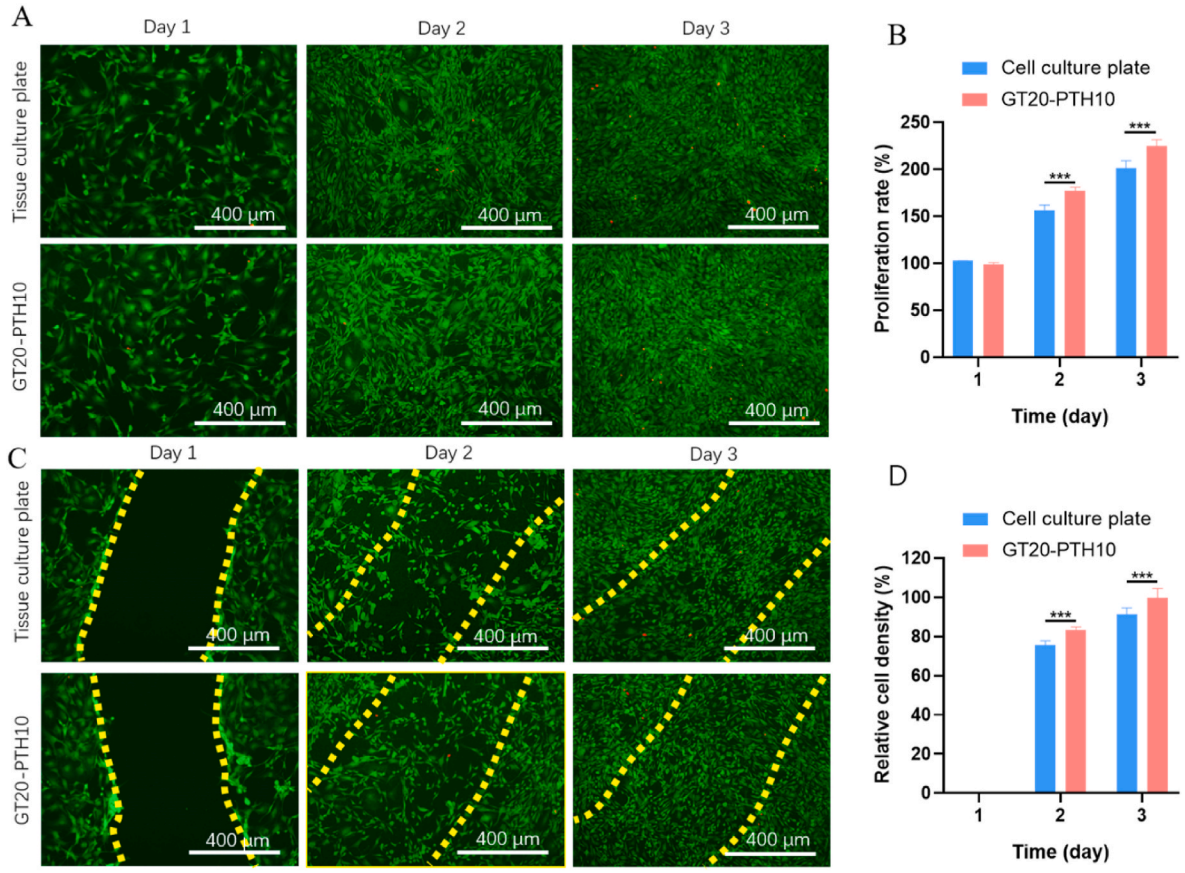

Fig. 4. A) Representative LIVE/DEAD images from MSCs seeded on tissue culture well-plate and GT20-PTH10 hydrogel surface. (Green: live cells; Red: dead cells) B) Quantification of cell proliferation rate on GT20-PTH10 hydrogel surface compared to tissue culture well plate after 1, 2, and 3 days of culture. C) Representative LIVE/DEAD images of MSCs grown on tissue culture well plate and GT20-PTH10 hydrogel at 1, 2, and 3 days after scratching. D) Quantification of relative cell densities migrated to the scratched area on GT20-PTH10 hydrogels and control samples, at days 1, 2, and 3.

deformation state, the nominal stress magnitude of the plug is 18.9 Pa. These findings are significant, because the approximate tensile stress for failure of the GT20-PTH10 hydrogel is 118 KPa, which is approximately four orders of magnitude larger than the maximum stress felt by the hydrogel plug. We also note that the final radial stretch will predict a higher stress magnitude than the radial stretch of $\lambda_r = 1.02$ corresponding to the physiological infusion volume of 0.1 mL.

After deformation the model is in a bi-axial stress state, where the hydrogel plug aligns with the x-y plane ($P_{xx} = P_{yy}$). Therefore, to examine the stresses on the adhesive plug and the interface between the

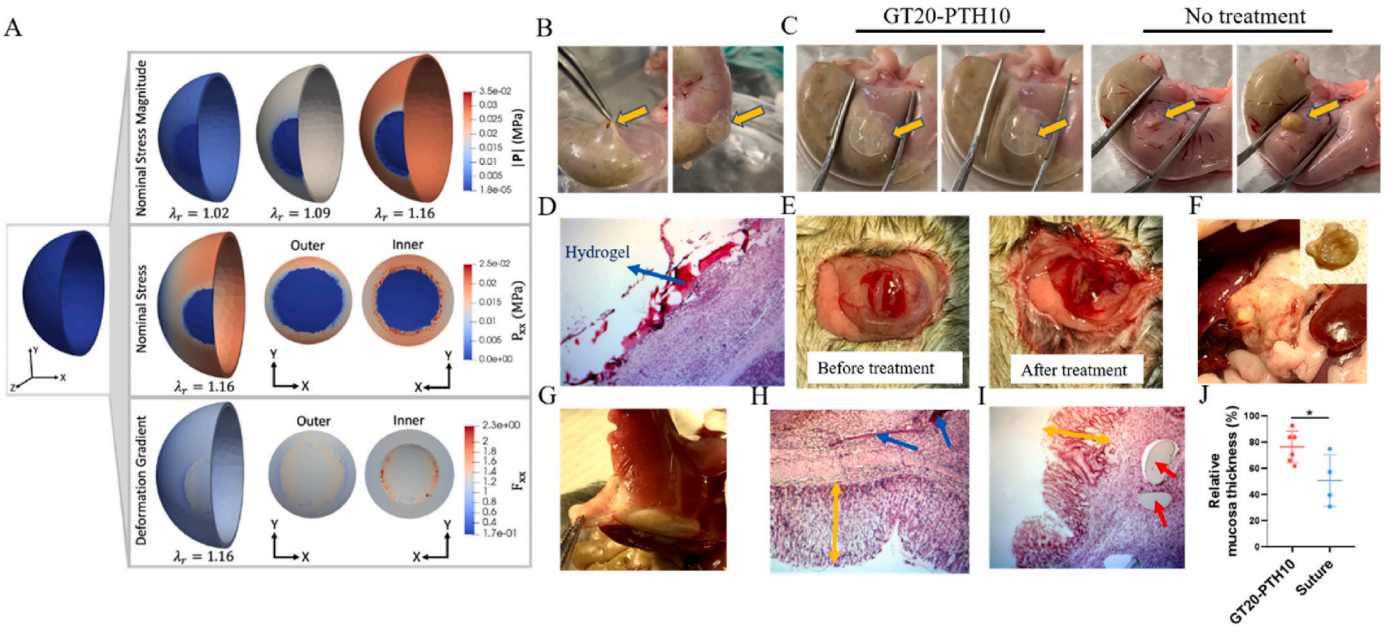

Fig. 5. A) (Top) Stress magnitude from unloaded to fully loaded state where displacement is applied to the inner surface until a final radial stretch of $\lambda_r = 1.16$ is achieved, where $\lambda_r = 1.02$ corresponds to an infusion volume of 0.1 mL (Middle) The sphere is in a biaxial stress state after deformation ($P_{xx} = P_{yy}$), with the adhesive plug aligning with the x-y plane. The stress interface between the native stomach and the adhesive material is displayed. (Bottom) The corresponding component of the deformation gradient ($F = I + \nabla u$). B) Representative images for creating a 5 mm hole on a rat stomach and blocking the hole with a GT20-PTH10 hydrogel plug. Representative images of a stomach C) treated with a GT20-PTH10 hydrogel plug (Left) and without any treatment (Right) before and after pressing with tweezers. D) H&E staining of GT20-PTH10 hydrogel plug sticking to a healthy mouse stomach surface after 10 days. E) Representative images of a perforated stomach before and after treatment of GT20-PTH10 hydrogel plug. Representative images of a perforated mouse stomach with treatment of a F) GT20-PTH10 hydrogel plug and G) suture after 10 days. H&E staining of H) GT20-PTH10 hydrogel plug and I) suture group after 10 days. Blue arrows point to the remaining hydrogels and the red ones point to the suture. Yellow arrows represent the mucosa thickness. J) Gastric mucosa thicknesses of GT20-PTH10 hydrogel and suture treatment groups. (n = 6 for the hydrogel group and n = 4 for the suture group).

two materials more closely, we display the principal nominal stress component in the x direction, P_{xx}. While the interface of the outer surface experiences lower stresses from $P_{xx} = 5 - 10$ KPa, the interface on the inner surface displays the maximum stresses of $P_{xx} = 25$ KPa. High interfacial stresses can contribute to de-adhesion of the hydrogel material from the native stomach tissue, but the maximum interfacial stress reported from our simulation is an order of magnitude smaller than the shear strength of 251 KPa for GT20-PTH10.

The deformation gradient component corresponding to the nominal stress component is shown where the deformation gradient quantifies the change between the reference/undeformed and deformed configuration (see supplemental). Corresponding to the highest stresses, the highest deformations also occur within the inner surface close to the interface. We note that the sphere with a perfect interface between materials represents a highly idealized geometry, and in the experiments there is some overlap of the hydrogel over the hole which likely contributes to better performance *in vivo*. The stretches of the GT20-PTH10 hydrogel are $\lambda_x = \lambda_y = 1.18$ and $\lambda_z = 0.71$ corresponding to strains of $\varepsilon_{xx} = \varepsilon_{yy} = 18\%$ and $\varepsilon_{zz} = -0.29\%$.

Following encouraging *in vitro* and simulation results, we first assessed the adhesion efficacy of our engineered GT20-PTH10 adhesive hydrogel ex vivo. After creating an approximately 5 mm diameter hole, gelatin (mixed with PTH) and TG (mixed with borax) were separately infused into a dual-syringe and incubated in a 37 °C water bath before being injected through a micro-mixer into the GP and solidifying as a plug to block the hole (Fig. 5B). After the GT20-PTH10 adhesive hydrogel plug was applied for a few minutes, we used tweezers to apply pressure to the stomach tissue. Fig. 5C and Video V4 show that no gastric content, including acid and food residue, leaked from the stomach, indicating strong adhesion between the stomach and the GT20-PTH10 adhesive hydrogel plug. However, a large amount of gastric content was squeezed out from stomachs without any treatment (Video V5).

Supplementary video related to this article can be found at https://doi.org/10.1016/j.bioactmat.2021.11.038

After this ex vivo treatment test, we investigated the adhesive properties of the GT20-PTH10 adhesive hydrogel plug *in vivo*. The GT20-PTH10 adhesive hydrogel plug was implanted on the surface of a healthy mouse stomach. After the hydrogel adhered to the stomach, saline was applied to the hydrogel surface to prevent tissue adhesion to other tissues or organs. With hydration layer, the hydrogel surface could play the role of lubrication. The results showed that the hydrogel plug tightly adhered to the stomach surface even with some degradation after 10 days (Fig. 5D). Meanwhile, when we applied the hydrogel plug to the GP site, bleeding was stopped (Fig. 5E), suggesting high adhesion of the hydrogel *in vivo*. Interestingly, no adhesion between other heathy organs and the stomach could be found after hydrogel plug treatment after 10 days (Fig. 5F), but severe tissues adhesion could be easily observed for suture treatment (Fig. 5G). Moreover, Fig. 5H also showed that the stomach inner mucosa surface was smooth and appeared intact after the GT20-PTH10 adhesive hydrogel treatment. Gastric mucus is a glycoprotein that serves two purposes: the lubrication of food masses to facilitate movement within the stomach and the formation of a protective layer over the lining epithelium of the stomach cavity. The GP defected areas exposed to corrosive gastric juice may induce a slow-healing of gastric mucosa, which results in patients suffering from this complication [41,42]. Therefore, whether or not the mucosa fully regenerates is a health hallmark of stomach after GP treatment [43,44]. The thickness of gastric mucosa following GT20-PTH10 adhesive hydrogel plugging was much higher than that of the suture group (Fig. 5H and I). The quantification of gastric mucosa thickness also confirmed this observation (Fig. 5J).

4. Conclusion

In summary, we report a novel adhesive hydrogel plug and demonstrate its potential use for gastric repair in mice. There are a few design principles that are worth reiterating. First, the hydrogel can be formed *in situ* so it is easy to apply and conforms to the GP site. Second, the hydrogel contains two synergistic networks: the gelatin network that is known to be bioactive and degradable and promote cell growth; the dynamically crosslinked PTH network dissipates energy and therefore enhances the toughness and adhesion strength of the hydrogel. Third, the hydrogel seals the GP tightly due to its strong adhesion to the tissues which may be attributed to both the high density of hydrogen bonds and the covalent bonds formed by free transglutaminase between the hydrogel and stomach tissues. Due to strong adhesiveness and toughness of the hydrogel, the plug could adhere to the GP site and withstand the peristaltic movement of the stomach during the healing process. With all these properties, the hydrogel plug effectively treated the GP and promoted mucosa regeneration in a mouse model. This study provides a proof of concept for the potential use of this hydrogel in developing GP treatments and as a bandage or plug for internal organ injury or defects.

Declaration of competing interest

The authors declare that they have no known competing financial interests or personal relationships that could have appeared to influence the work reported in this paper.

CRediT authorship contribution statement

Jing Chen: Conceptualization, Investigation, Methodology, Formal analysis, Writing – review & editing. **Julia S. Caserto:** Investigation, Writing – review & editing. **Ida Ang:** Formal analysis. **Kaavian Shariati:** Visualization. **James Webb:** Writing – review & editing. **Bo Wang:** Resources. **Xi Wang:** Resources. **Nikolaos Bouklas:** Formal analysis, Writing – review & editing. **Minglin Ma:** Supervision, Conceptualization, Visualization, Writing – review & editing.

Data availability

All data obtained from this study are included in the article or uploaded as supplementary information. The data that support the findings of this research are available from the corresponding authors upon reasonable request.

Acknowledgements

This work was partially supported by the Novo Nordisk Company, the Juvenile Diabetes Research Foundation (JDRF, 2-SRA-2018-472-S-B) and the Hartwell Foundation. This work made use of the Cornell Center for Materials Research Shared Facilities which are supported through the NSF MRSEC program (DMR-1719875).

Appendix A. Supplementary data

Supplementary data to this article can be found online at https://doi.org/10.1016/j.bioactmat.2021.11.038.

References

[1] K.T. Chung, V.G. Shelat, Perforated peptic ulcer-an update, World J. Gastroenterol. 9 (1) (2017) 1.
[2] K. Ramakrishnan, R.C. Salinas, Peptic ulcer disease, Am. Fam. Physician 76 (7) (2007) 1005–1012.
[3] W.I. Najm, Peptic ulcer disease, Prim. Care 38 (3) (2011) 383–394.
[4] L.E. Tolentino, N. Kallichanda, B. Javier, R. Yoshimori, S.W. French, A case report of gastric perforation and peritonitis associated with opportunistic infection by Sarcina ventriculi, Lab. Med. 34 (7) (2003) 535–537.
[5] S. Gupta, R. Kaushik, Peritonitis - the eastern experience, World J. Emerg. Surg. 1 (2006) 1–6.
[6] D. Nocca, R. Aggarwal, P. Blanc, B. Gallix, G.L. Di Mauro, B. Millat, C. Hons, E. Deneve, J.G. Rodier, G. Tincani, M.A. Pierredon, J.M. Fabre, Laparoseopic vertical banded gastroplasty - a multicenter prospective study of 200 procedures, Surg. Endosc. 21 (6) (2007) 870–874.
[7] W. Gossman, F. Tuma, B.G. Kamel, S. Cassaro, Gastric Perforation, StatPearls [Internet], StatPearls Publishing, 2019.
[8] M.J. Bertleff, J.F. Lange, Perforated peptic ulcer disease: a review of history and treatment, Dig, Surgery 27 (3) (2010) 161–169.
[9] J. Byun, H.Y. Kim, S.Y. Noh, S.H. Kim, S.E. Jung, S.C. Lee, K.W. Park, Neonatal gastric perforation: a single center experience, World J. Gastroenterol. 6 (8) (2014) 151.
[10] I. Michelet, F. Agresta, Perforated peptic ulcer: laparoscopic approach, Eur. J. Surg. 166 (5) (2000) 405–408.
[11] S. Glüer, A.I. Schmidt, N.K. Jesch, B.M. Ure, Laparoscopic repair of neonatal gastric perforation, J. Pediatr. Surg. 41 (1) (2006) e57–e58.
[12] R. Shin, S.M. Lee, B. Sohn, D.W. Lee, I. Song, Y.J. Chai, H.W. Lee, H.S. Ahn, I. M. Jung, J.K. Chung, Predictors of morbidity and mortality after surgery for intestinal perforation, Ann. Coloproctol. 32 (6) (2016) 221.
[13] C. Svanes, Trends in perforated peptic ulcer: incidence, etiology, treatment, and prognosis, World J. Surg. 24 (3) (2000) 277–283.
[14] E.S. Sani, A. Kheirkhah, D. Rana, Z. Sun, W. Foulsham, A. Sheikhi, A. Khademhosseini, R. Dana, N. Annabi, Sutureless repair of corneal injuries using naturally derived bioadhesive hydrogels, Sci. Adv. 5 (3) (2019), eaav1281.
[15] H. Yuk, C.E. Varela, C.S. Nabzdyk, X. Mao, R.F. Padera, E.T. Roche, X. Zhao, Dry double-sided tape for adhesion of wet tissues and devices, Nature 575 (7781) (2019) 169–174.
[16] G.M. Taboada, K. Yang, M.J. Pereira, S.S. Liu, Y. Hu, J.M. Karp, N. Artzi, Y. Lee, Overcoming the translational barriers of tissue adhesives, Nat. Rev. Mater. (2020) 1–20.
[17] S. Tanaka, K. Kanetaka, M. Fujii, S. Ito, Y. Sakai, S. Kobayashi, K. Yamanouchi, F. Fujita, T. Kuroki, S. Eguchi, Cell sheet technology for the regeneration of gastrointestinal tissue using a novel gastric perforation rat model, Surg. Today 47 (1) (2017) 114–121.
[18] R. Matsumoto, K. Kanetaka, Y. Maruya, S. Yamaguchi, S. Kobayashi, D. Miyamoto, K. Ohnita, Y. Sakai, K. Hashiguchi, K. Nakao, The efficacy of autologous myoblast sheet transplantation to prevent perforation after duodenal endoscopic submucosal dissection in porcine model, Cell Transplant. 29 (2020), 0963689720963882.
[19] T. Ohki, M. Yamato, M. Ota, R. Takagi, D. Murakami, M. Kondo, R. Sasaki, H. Namiki, T. Okano, M. Yamamoto, Prevention of esophageal stricture after endoscopic submucosal dissection using tissue-engineered cell sheets, Gastroenterology 143 (3) (2012) 582–588, e2.
[20] C. Cui, T. Wu, X. Chen, Y. Liu, Y. Li, Z. Xu, C. Fan, W. Liu, A janus hydrogel wet adhesive for internal tissue repair and anti-postoperative adhesion, Adv. Funct. Mater. 30 (49) (2020) 2005689.
[21] W. Wang, Z. Zeng, L. Xiang, C. Liu, D. Diaz-Dussan, Z. Du, A.B. Asha, W. Yang, Y.-Y. Peng, M. Pan, R. Narain, J. Liu, H. Zeng, Injectable self-healing hydrogel via biological environment-adaptive supramolecular assembly for gastric perforation healing, ACS Nano 15 (6) (2021) 9913–9923.
[22] X. Peng, X.F. Xia, X.Y. Xu, X.F. Yang, B.G. Yang, P.C. Zhao, W.H. Yuan, P.W. Y. Chiu, L.M. Bian, Ultrafast self-gelling powder mediates robust wet adhesion to promote healing of gastrointestinal perforations, Sci. Adv. 7 (23) (2021) 13.
[23] D.R. Griffin, M.M. Archang, C.H. Kuan, W.M. Weaver, J.S. Weinstein, A.C. Feng, A. Ruccia, E. Sideris, V. Ragkousis, J. Koh, M.V. Plikus, D. Di Carlo, T. Segura, P. O. Scumpia, Activating an adaptive immune response from a hydrogel scaffold imparts regenerative wound healing, Nat. Mater. 20 (4) (2021) 560–569.
[24] C.C.L. Schuurmans, M. Mihajlovic, C. Hiemstra, K. Ito, W.E. Hennink, T. Vermonden, Hyaluronic acid and chondroitin sulfate (meth)acrylate-based hydrogels for tissue engineering: synthesis, characteristics and pre-clinical evaluation, Biomaterials 268 (2021) 24.
[25] S. Khosravimelal, M. Mobaraki, S. Eftekhari, M. Ahearne, A.M. Seifalian, M. Gholipourmalekabadi, Hydrogels as Emerging Materials for Cornea Wound Healing, Small 2006335.
[26] X. Xu, X. Xia, K. Zhang, A. Rai, Z. Li, P. Zhao, K. Wei, L. Zou, B. Yang, W.-K. Wong, P.W.-Y. Chiu, L. Bian, Bioadhesive hydrogels demonstrating pH-independent and ultrafast gelation promote gastric ulcer healing in pigs, Sci. Transl. Med. 12 (558) (2020).
[27] T. Zhang, H. Yuk, S. Lin, G.A. Parada, X. Zhao, Tough and tunable adhesion of hydrogels: experiments and models, Acta Mech. Sin. 33 (3) (2017) 543–554.
[28] J. Chen, D. Wang, L.H. Wang, W.J. Liu, A. Chiu, K. Shariati, Q.S. Liu, X. Wang, Z. Zhong, J. Webb, R.E. Schwartz, N. Bouklas, M.L. Ma, An adhesive hydrogel with "Load-Sharing" effect as tissue bandages for drug and cell delivery, Adv. Mater. 32 (43) (2020) 2001628.
[29] E. Shirzaei Sani, R. Portillo-Lara, A. Spencer, W. Yu, B.M. Geilich, I. Noshadi, T. J. Webster, N. Annabi, Engineering adhesive and antimicrobial hyaluronic acid/elastin-like polypeptide hybrid hydrogels for tissue engineering applications, ACS Biomater. Sci. Eng. 4 (7) (2018) 2528–2540.
[30] D.L. Gan, W.S. Xing, L.L. Jiang, J. Fang, C.C. Zhao, F.Z. Ren, L.M. Fang, K.F. Wang, X. Lu, Plant-inspired adhesive and tough hydrogel based on Ag-Lignin nanoparticles-triggered dynamic redox catechol chemistry, Nat. Commun. 10 (1) (2019) 1–10.
[31] X. Wang, K.G. Maxwell, K. Wang, D.T. Bowers, J.A. Flanders, W.J. Liu, L.H. Wang, Q.S. Liu, C.Y. Liu, A. Naji, Y. Wang, B. Wang, J. Chen, A.U. Ernst, J.M. Melero-Martin, J.R. Millman, M.L. Ma, A nanofibrous encapsulation device for safe

delivery of insulin-producing cells to treat type 1 diabetes, Sci. Transl. Med. 13 (596) (2021) 18.
[32] J. Zhao, D. Liao, H. Gregersen, Tension and stress in the rat and rabbit stomach are location- and direction-dependent, Neuro Gastroenterol. Motil. 17 (3) (2005) 388–398.
[33] M. Alnæs, J. Blechta, J. Hake, A. Johansson, B. Kehlet, A. Logg, C. Richardson, J. Ring, M. Rognes, G. Wells, Archive of Numerical Software: the FEniCS Project Version 1.5, University Library Heidelberg, 2015.
[34] A. Logg, K.-A. Mardal, G. Wells, Automated Solution of Differential Equations by the Finite Element Method: the FEniCS Book, Springer Science & Business Media, 2012.
[35] K.-B. Bae, S.-H. Kim, S.-J. Jung, K.-H. Hong, Cyanoacrylate for colonic anastomosis; is it safe? Int. J. Colorectal Dis. 25 (5) (2010) 601–606.
[36] T. Vuocolo, R. Haddad, G.A. Edwards, R.E. Lyons, N.E. Liyou, J.A. Werkmeister, J. A. Ramshaw, C.M. Elvin, A highly elastic and adhesive gelatin tissue sealant for gastrointestinal surgery and colon anastomosis, J. Gastrointest. Surg. 16 (4) (2012) 744–752.
[37] Y. Yang, J. Zhang, Z. Liu, Q. Lin, X. Liu, C. Bao, Y. Wang, L. Zhu, Tissue-integratable and biocompatible photogelation by the imine crosslinking reaction, Adv. Mater. 28 (14) (2016) 2724–2730.
[38] S. Liang, Y. Zhang, H. Wang, Z. Xu, J. Chen, R. Bao, B. Tan, Y. Cui, G. Fan, W. Wang, Paintable and rapidly bondable conductive hydrogels as therapeutic cardiac patches, Adv. Mater. 30 (23) (2018) 1704235.
[39] M. Xie, J. Li, S. Zhang, D. Zhu, X. Mei, Z. Wang, X. Cheng, Z. Li, S. Wang, K. Cheng, A trifunctional contraceptive gel enhances the safety and quality of sexual intercourse, Bioact. Mater. 6 (6) (2021) 1777–1788.
[40] S. Zhang, D. Zhu, X. Mei, Z. Li, J. Li, M. Xie, H.J.W. Xie, S. Wang, K. Cheng, Advances in biomaterials and regenerative medicine for primary ovarian insufficiency therapy, Bioact. Mater. 6 (7) (2021) 1957–1972.
[41] M. Wang, Y.-Q. Li, J. Cao, M. Gong, Y. Zhang, X. Chen, M.-X. Tian, H.-Q. Xie, Accelerating effects of genipin-crosslinked small intestinal submucosa for defected gastric mucosa repair, J. Mater. Chem. B 5 (34) (2017) 7059–7071.
[42] S. Hauck, P. Zager, N. Halfter, E. Wandel, M. Torregrossa, A. Kakpenova, S. Rother, M. Ordieres, S. Räthel, A. Berg, Collagen/hyaluronan based hydrogels releasing sulfated hyaluronan improve dermal wound healing in diabetic mice via reducing inflammatory macrophage activity, Bioact. Mater. 6 (12) (2021) 4342–4359.
[43] C. Atuma, V. Strugala, A. Allen, L. Holm, The adherent gastrointestinal mucus gel layer: thickness and physical state in vivo, Am. J. Physiol. Gastrointest. Liver Physiol. 280 (5) (2001) G922–G929.
[44] P. Vasconcelos, H. Kushima, M. Andreo, C.A. Hiruma-Lima, W. Vilegas, R. K. Takahira, C. Pellizzon, Studies of gastric mucosa regeneration and safety promoted by Mouriri pusa treatment in acetic acid ulcer model, J. Ethnopharmacol. 115 (2) (2008) 293–301.